RSC Advances

ROYAL SOCIETY OF CHEMISTRY

www.rsc.org/advances

Graphical Abstract

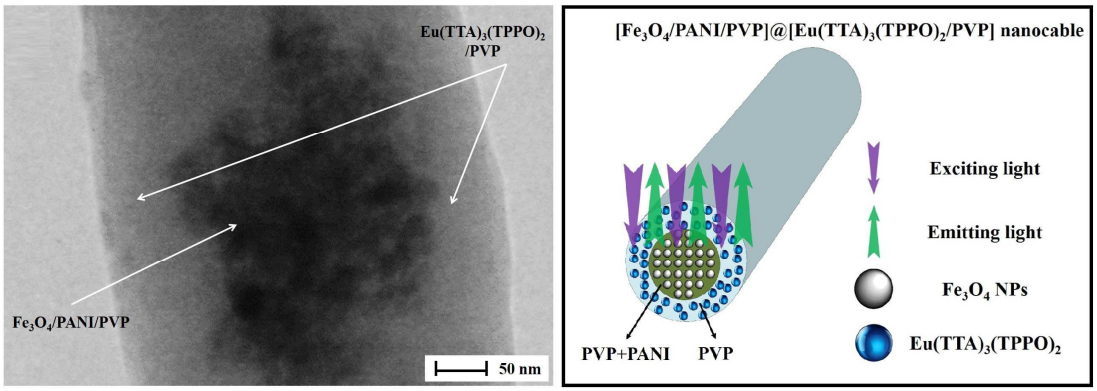

A new nanostructure of luminescent-electrical-magnetic trifunctional nanocables has been successfully fabricated by specially designed coaxial spinnerets electrospinning technology. Upon the unique feature of the core-shell coaxial nanostructure, nanocables can help to realize effective isolating rare earth complexes from the dark-colored PANI and Fe_3O_4 NPs to ultimately reduce the impact of PANI and Fe_3O_4 NPs on fluorescent property of the nanofibers, and thus strong luminescence of the luminescent-electrical-magnetic nanocables can be achieved.

Journal Name

ARTICLE

Direct Electrospinning Construction of Nanocables with Electrical Conductive-Magnetic Core and Insulative-Photoluminescent Sheath

Received 00th January 20xx,
Accepted 00th January 20xx

DOI: 10.1039/x0xx00000x

www.rsc.org/

Lei Han, Qianli Ma, Xiangting Dong*[a]

Novel flexible luminescent-electrical-magnetic trifunctional nanocables have been successfully fabricated by specially designed coaxial spinnerets electrospinning technology. Europium complex $Eu(TTA)_3(TPPO)_2$ (TTA=2-Thenoyltrifluoroacetone, TPPO=Triphenylphosphine oxide), PANI and Fe_3O_4 nanoparticles (NPs) were respectively incorporated into polyvinyl pyrrolidone (PVP) and electrospun into nanocables with Fe_3O_4/PANI/PVP as core and $Eu(TTA)_3(TPPO)_2$/PVP as the sheath. The morphology and properties of the final products were investigated in detail by X-ray diffractometry (XRD), scanning electron microscopy (SEM), transmission electron microscopy (TEM), fluorescence spectroscopy, Hall effect measurement system and vibrating sample magnetometer (VSM). SEM observation indicates that the diameter of the nanocables is 414±13 nm. TEM analysis shows the core diameter is *ca.* 250 nm containing magnetic nanoparticles and polyaniline, and the sheath thickness is *ca.* 81 nm. Fluorescence emission peaks of Eu^{3+} ions in the [Fe_3O_4/PANI/PVP]@[$Eu(TTA)_3(TPPO)_2$/PVP] nanocables are observed and assign to the energy levels transitions of $^5D_0 \rightarrow {}^7F_0$ (579 nm), $^5D_0 \rightarrow {}^7F_1$ (592 nm), $^5D_0 \rightarrow {}^7F_2$ (614 nm), and the $^5D_0 \rightarrow {}^7F_2$ hypersensitive transition at 614 nm is the dominant emission peak. The obtained nanocables possess better fluorescent intensity than their counterpart Fe_3O_4/PANI/$Eu(TTA)_3(TPPO)_2$/PVP composite nanofibers. The electrical conductivity of the core of nanocable reaches up to the order of 10^{-3} $S \cdot cm^{-1}$. The luminescent intensity, electrical conductivity and magnetic properties of the nanocables can be tunable by adjusting various amounts of rare earth complex, PANI and Fe_3O_4 NPs. The [Fe_3O_4/PANI/PVP]@[$Eu(TTA)_3(TPPO)_2$/PVP] flexible luminescent-electrical-magnetic trifunctional nanocables have potential applications in molecular electronics, biomedicine, microwave absorption and display device owing to their excellent multifunctionality.

1 Introduction

Recently, multifunctional nanomaterials have attracted much interest of scientists, since they provide the possibility for multifunctional properties and enhanced functionality in contrast to their more-limited single functional nanomaterials[1-3]. For instance, magnetic-photoluminescent bifunctional nanomaterials have wide applications in the fields of targeted drug delivery[4, 5], controllable drug release[6, 7] and bioimaging[8-10] due to their special property in magnetic resonance and fluorescent probe. Luminescent-electrical-magnetic trifunctional micro/nanostructures are of special interest owing to their potential applications in areas such as molecular electronics[11], biomedicine[12] and electromagnetic interference shielding[13].

Multifunctional nanomaterials can acquire optimized optical, electrical, magnetic, and biological properties by effectively combining the respective function of different component. Fe_3O_4 nanoparticles (NPs) are the most widely studied magnetic nanoparticles not only for the fundamental magnetic properties[14], but also for biomedical applications[15-17]. It is well known that polyaniline (PANI), as one of the most conducting polymers, has been extensively explored and used in many areas such as electrochromic devices, secondary batteries, catalysis and biosensors[18-20] owing to its good electrical conductivity, reversible redox property and good environmental stability[21]. Europium complexes[22, 23] have excellent luminescent properties owing to the antenna effect of ligands and the f-f electron transition of Eu^{3+} ions, resulting in important applications in biological labelling[24], electroluminescent devices[25] and laser[26].

Electrospinning is a simple and effective method to fabricate one-dimensional micro- and nanomaterials. polyvinyl pyrrolidone (PVP) has been widely used for electrospinning owing to its good solubility, high flexibility, non-toxicity, easy

[a] Key Laboratory of Applied Chemistry and Nanotechnology at Universities of Jilin Province, Changchun University of Science and Technology, Changchun 130022. Fax: 86 0431 85383815; Tel: 86 0431 85582575; E-mail: dongxiangting888@163.com.

obtainment, low costs, etc[27]. By using PVP as template, one-dimensional nanomaterials with various morphologies have been successfully prepared via electrospinning technique, such as nanofibers[28-30], hollow nanofibers[31, 32], nanobelts[33], nanocables[34], etc. And some preparations of one-dimensional luminescent-electrical-magnetic multifunctional materials have been reported by using the above method, such as, magnetic-fluorescent bifunctional composite nanofibers[35], photoluminescence-electrical conduction bifunctional composite nanofibers[36], as well as photoluminescence-electricity-magnetism trifunctional composite nanofibers[37], composite nanobelts[27]. On the basis of these studies, the nanocomposites suffered heavy losses in fluorescent intensity when Fe_3O_4 NPs and PANI were directly blended with the rare earth luminescent compounds. Therefore, rare earth luminescent compounds should be effectively isolated from Fe_3O_4 NPs and PANI to avoid direct contact. Up to now, some types of nanocables have been synthesized. The researchers have adopted carbon fibers or tubes, metals, conductive polymers and other conductive materials as the inner conductor of nanocables[38, 39]. The sheath must have good insulation property and, sometimes, have other functions. Inspired by the structure of nanocable, in this work, we designed and fabricated novel nanocable composed of a Fe_3O_4 NPs/PANI/polyvinyl pyrrolidone (PVP) core and a Eu complexes/PVP sheath. By constructing such kind of structure, luminescent compounds can be effectively isolated from Fe_3O_4 NPs and PANI to avoid direct contact. Furthermore, it is the first time that the electrically conductive nanocables were endowed with tunable luminescence-magnetism properties. The structure, conductivity, fluorescence, and magnetism of the coaxial conductive nanocables were studied, and some new results were obtained.

2 Experimental

2.1 Chemicals

Polyvinyl pyrrolidone (PVP, Mw ≈ 90,000), europium oxide (Eu_2O_3 99.99%), 2-Thenoyltrifluoroacetone (TTA), triphenylphosphine oxide (TPPO) and dimethylformamide (DMF) were bought from Tianjin Tiantai Fine Chemical Co., Ltd. $FeCl_3·6H_2O$, $FeSO_4·7H_2O$, NH_4NO_3, polyethyleneglycol (PEG, Mw ≈ 20,000), ammonia, anhydrous ethanol, aniline (ANI), and (IS)-(+)-Camphor-10 sulfonic acid (CSA) were bought from Sinopharm Chemical Reagent Co., Ltd. Ammonium persulfate was purchased from Guangdong Xilong Chemical Co., Ltd. All the reagents were of analytical grade and used directly as received without further purification.

2.2 Preparation of oleic acid modified Fe_3O_4 nanoparticles by coprecipitation method

Monodispersed Fe_3O_4 NPs with a narrow size distribution were prepared by using the chemical co-precipitation method. In order to prevent the particles from aggregating, PEG was used as the protective agent. In a typical procedure, 5.4060 g (0.0200 mol) of $FeCl_3·6H_2O$, 2.7800 g (0.0100 mol) of $FeSO_4·7H_2O$, 4.0022 g (0.0500 mol) of NH_4NO_3 and 1.9000 g of PEG were added into 100 mL of deionized water to form a uniform solution under the protection of argon atmosphere with vigorous stirring at 50 °C. After the mixture had been bubbled with argon for 30 min, 0.1 $mol·L^{-1}$ of $NH_3·H_2O$ was dropwise added into the mixture until the pH value was above 11. Black precipitates were formed quickly, and the resultant suspension was kept stirring for another 30 min under argon at 50 °C. Subsequently, the product was separated by using a magnet and washed with distilled water three times, and then dried in an electric vacuum oven at 60 °C for 12 h. The size distribution of the as-prepared Fe_3O_4 NPs is almost uniform, and the diameter of the nanoparticles is 8-10 nm.

To improve the monodispersity, stability and solubility of Fe_3O_4 NPs in the spinning solution, the as-prepared Fe_3O_4 NPs were then coated with oleic acid (OA) as below: 2.0000 g of the as-prepared Fe_3O_4 NPs were ultrasonically dispersed in 100 mL of deionized water for 20 min. The suspension was heated to 80 °C under argon atmosphere with vigorous mechanical stirring for 30 min and then 1 mL of OA was dropwise added. Reaction was stopped after heating and stirring the mixture for 40 min. The precipitates were collected from the solution by magnetic separation, washed with ethyl alcohol for three times, and then dried in an electric vacuum oven at 60 °C for 6 h. Thus, oleic acid modified Fe_3O_4 nanoparticles (Fe_3O_4 NPs@OA) were synthesized. The TEM images of the Fe_3O_4 NPs before and after coating OA are provided in the Electronic Supplementary Information.

2.3 Synthesis of $Eu(TTA)_3(TPPO)_2$ complexes

$Eu(TTA)_3(TPPO)_2$ powder was synthesized according to the traditional method as described in reference[40]. 1.7596 g (5.0000 mmol) of Eu_2O_3 was dissolved in 10 mL of concentrated nitric acid and then crystallized by evaporation of excess nitric acid and water, and 3.3798 g (10.0000 mmol) of $Eu(NO_3)_3$ was acquired. $Eu(NO_3)_3$ ethanol solution was prepared by adding 20 mL of anhydrous ethanol into the above $Eu(NO_3)_3$. 6.6670 g (30.0000 mmol) of HTTA and 5.5680 g (20.0000 mmol) of TPPO were dissolved in 200 mL of ethanol. The $Eu(NO_3)_3$ solution was then added into the mixture solution of TTA and TPPO with magnetic agitation for 3 h at 60 °C. The precipitate was collected by filtration and then dried at 60 °C for 12 h.

2.4 Fabrication of $Eu(TTA)_3(TPPO)_2$/PVP nanofibers

In order to find the optimum mass ratio of $Eu(TTA)_3(TPPO)_2$ to PVP, a series of $Eu(TTA)_3(TPPO)_2$/PVP nanofibers were fabricated by traditional uniaxial electrospinning setup at room temperature under a positive high voltage of 16 kV, the distance between the spinneret and the collector was fixed to 18 cm, and relative humidity was 44-48 %. The compositions of

these spinning solutions were 4.5000 g of DMF, 1.0000 g of PVP and certain amounts of $Eu(TTA)_3(TPPO)_2$ powder. The mass percentages of $Eu(TTA)_3(TPPO)_2$ to PVP were 15 % (0.1500 g (0.1091 mmol) of $Eu(TTA)_3(TPPO)_2$), 20 % (0.2000 g (0.1454 mmol) of $Eu(TTA)_3(TPPO)_2$), 25 % (0.2500 g (0.1818 mmol) of $Eu(TTA)_3(TPPO)_2$), 30 % (0.3000 g (0.2182 mmol) of $Eu(TTA)_3(TPPO)_2$) and 35 % (0.3500 g (0.2545 mmol) of $Eu(TTA)_3(TPPO)_2$), respectively.

2.5 Fabrication of luminescent-electrical-magnetic trifunctional nanocables *via* electrospinning

In the preparation of inner electrospinning spinning solution, ANI was dissolved in 7.0000 g DMF, then Fe_3O_4 NPs were ultrasonically dispersed into the DMF solution for 15 min, and then PVP and CSA were slowly added into the above solution with magnetic stirring. The mixture was then cooled down to 0 °C in an ice-bath. Ammonium persulfate (APS) was used as an oxidant and dispersed into 6.0000 g DMF at 0 °C and then added dropwise into the above mixture with magnetic stirring, the molar ratio of ANI, CSA and APS was 2:1:2. The mixture was allowed to react for 24 h at 0 °C and PANI was obtained by the polymerization of aniline. The final mixture was denoted as spinning solution I. In the preparation of outer electrospinning spinning solution, A mixed solution of $Eu(TTA)_3(TPPO)_2$, PVP and DMF was prepared as the spinning solution II. The dosages of these materials were summarized in Table 1 and Table 2.

Table 1 Compositions of the spinning solution I

Spinning solutions I	Compositions				
	ANI /g	CSA /g	APS /g	Fe_3O_4 /g	PVP /g
S1	0.4500	0.5600	1.1030	1.5000	1.5000
S2	0.6000	0.7473	0.4700	1.5000	1.5000
S3	0.7500	0.9336	1.8400	1.5000	1.5000
S4	0.6000	0.7473	0.4700	3.0000	1.5000
S5	0.6000	0.7473	0.4700	4.5000	1.5000

Table 2 Compositions of the spinning solution II

Spinning solution II	Compositions		
	$Eu(TTA)_3(TPPO)_2$ /g	PVP /g	DMF /g
S6	0.2500	1.0000	5.5000

Homemade coaxial spinnerets was used in this study and the electrospinning setup was indicated in Fig. 1. Spinning solution I was injected into the inner syringe while the spinning solution II was loaded into the outer one. A flat iron net was used as a collector and put about 18 cm away from the spinneret. A positive direct current (DC) voltage of 16 kV was applied between the spinneret and the collector to generate stable, continuous PVP-based nanocables under the ambient temperature of 20-24 °C and the relative humidity of 44-48 %.

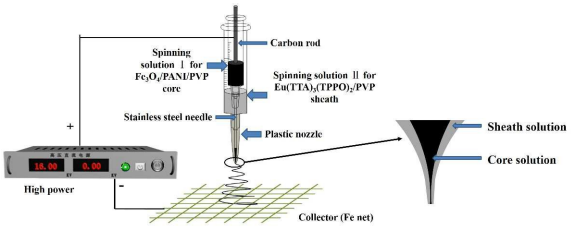

Fig. 1 Schematic diagram of the homemade coaxial electrospinning spinneret and the electrospinning setup, in which the inset shows the detail of coaxial Taylor cone

2.6 Fabrication of Fe_3O_4/PANI/$Eu(TTA)_3(TPPO)_2$/PVP composite nanofibers

Fe_3O_4/PANI/$Eu(TTA)_3(TPPO)_2$/PVP composite nanofibers, as a contrast sample, were also fabricated by mixing spinning solution S2 and spinning solution S6 together at the volume ratio of 1:1 and electrospun using traditional uniaxial electrospinning method to study the superiority of the structure of nanocables. The other spinning parameters were the same as those were in the fabrication of nanocables.

2.7 Characterization methods

Phase analysis of the as-prepared Fe_3O_4 NPs and [Fe_3O_4/PANI/PVP]@[$Eu(TTA)_3(TPPO)_2$/PVP] nanocables was performed by an X-ray powder diffractometer (XRD, Bruker, D8 FOCUS) with Cu Ka radiation (λ= 0.15406 nm) and Ni filter, the operation current and voltage were maintained at 20 mA and 40 kV, and scanning speed, step length and diffraction range were settled as 10 °·min^{-1}, 0.1 °·s^{-1} and 10-80 °, respectively. The morphology and internal structure of [Fe_3O_4/PANI/PVP]@[$Eu(TTA)_3(TPPO)_2$/PVP] nanocables were observed by a field emission scanning electron microscope (SEM, XL-30) and a transmission electron microscope (TEM, JEM-2010), respectively. The measurements of photoluminescence (PL) spectra and the luminescence decay curves were carried out by a HITACHI F-7000 fluorescence spectrophotometer using a 150 W Xe lamp as the excitation source, and scanning speed was fixed at 1200 nm·min^{-1}. Then, the magnetic performance of Fe_3O_4 NPs@OA and nanocables were measured by a vibrating sample magnetometer (VSM, MPMS SQUID XL). The conductive property was detected by Hall effect measurement system (ECOPIA HMS-3000). The ultraviolet-visible spectra of samples were determined by a UV-1240 ultraviolet-visible spectrophotometer. All the measures were performed at room temperature.

3 Results and discussion

3.1 Characterizations of the structure and morphology

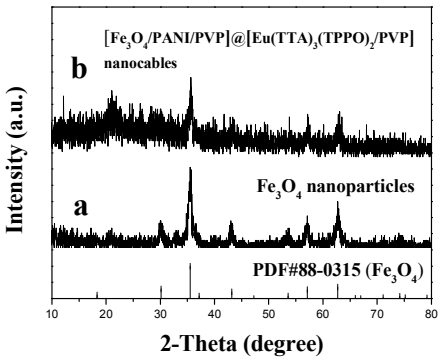

Fig. 2 XRD patterns of Fe_3O_4 nanoparticles (a) and $[Fe_3O_4/PANI/PVP]@[Eu(TTA)_3(TPPO)_2/PVP]$ nanocables (S4@S6) (b) with the PDF standard card of Fe_3O_4

The phase compositions of the Fe_3O_4 nanoparticles (Fig. 2a) and $[Fe_3O_4/PANI/PVP]@[Eu(TTA)_3(TPPO)_2/PVP]$ nanocables (Fig. 2b) were characterized by means of XRD analysis, as shown in Fig. 2. It can be seen that the XRD patterns of the as-prepared Fe_3O_4 nanoparticles conform to the cubic structure of Fe_3O_4 (PDF 88-0315), and no characteristic peaks are observed for other impurities such as Fe_2O_3 and FeO(OH). The XRD analysis result of $[Fe_3O_4/PANI/PVP]@[Eu(TTA)_3(TPPO)_2/PVP]$ nanocables (S4@S6) demonstrates that the nanocables contain Fe_3O_4 nanoparticles, and the diffraction peak of the amorphous PVP and PANI ($2\theta = 22.2°$)[41] also could be observed.

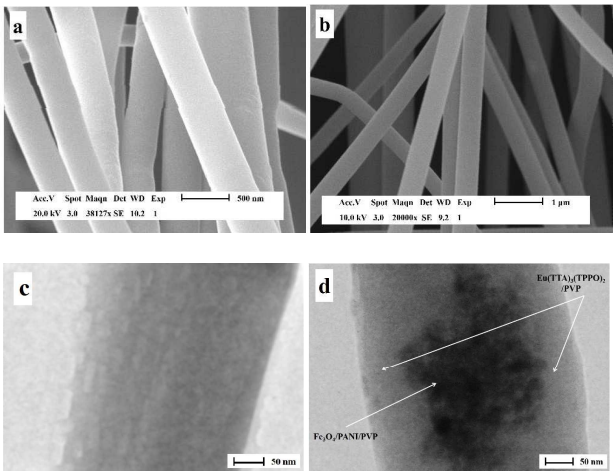

Fig. 3 SEM images of $Eu(TTA)_3(TPPO)_2/PVP$ nanofibers (a) and $[Fe_3O_4/PANI/PVP]@[Eu(TTA)_3(TPPO)_2/PVP]$ nanocables (S4@S6) (b); TEM images of $Eu(TTA)_3(TPPO)_2/PVP$ nanofibers (c) and $[Fe_3O_4/PANI/PVP]@[Eu(TTA)_3(TPPO)_2/PVP]$ nanocables (S4@S6) (d)

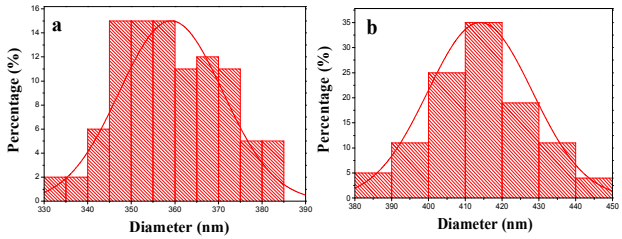

Fig. 4 Histograms of diameters of $Eu(TTA)_3(TPPO)_2/PVP$ nanofibers (a) and $[Fe_3O_4/PANI/PVP]@[Eu(TTA)_3(TPPO)_2/PVP]$ nanocables (S4@S6) (b)

The morphology and structure of $Eu(TTA)_3(TPPO)_2/PVP$ nanofibers and $[Fe_3O_4/PANI/PVP]@[Eu(TTA)_3(TPPO)_2/PVP]$ nanocables (S4@S6) were characterized by the combination of SEM and TEM. The SEM images of $Eu(TTA)_3(TPPO)_2/PVP$ nanofibers and $[Fe_3O_4/PANI/PVP]@[Eu(TTA)_3(TPPO)_2/PVP]$ nanocables shown in Fig. 3a and 3b demonstrate that the as-prepared nanofibers and nanocables are relatively smooth. The diameters of $Eu(TTA)_3(TPPO)_2/PVP$ nanofibers and $[Fe_3O_4/PANI/PVP]@[Eu(TTA)_3(TPPO)_2/PVP]$ nanocables are respectively 359±12 nm and 414±13 nm under the confidence level of 95 % (Fig. 4a and 4b).

The TEM images of $Eu(TTA)_3(TPPO)_2/PVP$ nanofibers and $[Fe_3O_4/PANI/PVP]@[Eu(TTA)_3(TPPO)_2/PVP]$ nanocables (S4@S6) are respectively presented in Fig. 3c and 3d. As seen in Fig. 3c, no particle can be observed in the amorphous $Eu(TTA)_3(TPPO)_2/PVP$ nanofibers. Of the $[Fe_3O_4/PANI/PVP]@[Eu(TTA)_3(TPPO)_2/PVP]$ nanocables (S4@S6), the core contains large number of nanoparticles, and the sheath is amorphous. The diameter of the core containing magnetic nanoparticles and polyaniline is *ca.* 250 nm and the sheath thickness is *ca.* 81 nm. A slightly magnetic agglomeration phenomenon can be seen from the TEM image. The Fe_3O_4 nanoparticles are only scattered in the core of the nanocables, indicating that $Fe_3O_4/PANI/PVP$ was successfully coated with $Eu(TTA)_3(TPPO)_2/PVP$ and a coaxial structure was formed. The SEM and TEM images of the other $[Fe_3O_4/PANI/PVP]@[Eu(TTA)_3(TPPO)_2/PVP]$ nanocables samples are provided in the Electronic Supplementary Information.

3.2 Photoluminescence (PL) property

In order to obtain the optimum mass percentage of $Eu(TTA)_3(TPPO)_2$ to PVP, a series of $Eu(TTA)_3(TPPO)_2/PVP$ nanofibers were fabricated and analyzed. As shown in Fig. 5, the luminescent intensity is increased at the beginning and then decreases with adding more $Eu(TTA)_3(TPPO)_2$. The highest value occurs when the mass percentage of $Eu(TTA)_3(TPPO)_2$ to PVP is 25 %. Fig. 5(a) demonstrates the excitation spectra of the samples. Broad excitation bands extending from 200 to 400 nm are observed when monitoring wavelength is 614 nm in various samples. The peak at 364 nm assigned to the $\pi \rightarrow \pi^*$ electron transition of the ligands could be also identified. As shown in Fig. 5(b), characteristic emission peaks of Eu^{3+} are observed under excitation of 364-nm ultraviolet light and ascribed to the energy levels transitions of $^5D_0 \rightarrow {}^7F_0$ (579 nm), $^5D_0 \rightarrow {}^7F_1$ (592 nm), $^5D_0 \rightarrow {}^7F_2$ (614 nm) and the $^5D_0 \rightarrow {}^7F_2$ hypersensitive transition at 614 nm is the predominant emission peak. The results indicates that the composite nanofibers containing 25 % $Eu(TTA)_3(TPPO)_2$ have the strongest fluorescence intensity. The RE complex-doped polymers have an optimum content of RE complexes in most cases. When the doping concentration of the RE complexes exceeds the

optimum content, the fluorescence intensity of the RE complex-doped polymer usually decreases due to quenching[35]. The quenching concentration of $Eu(TTA)_3(TPPO)_2$ is determined to be 25 %. Therefore, the mass percentage of $Eu(TTA)_3(TPPO)_2$ to PVP as 25 % was adopted to prepare $[Fe_3O_4/PANI/PVP]@[Eu(TTA)_3(TPPO)_2/PVP]$ nanocables and $Fe_3O_4/PANI/Eu(TTA)_3(TPPO)_2/PVP$ composite nanofibers thereafter.

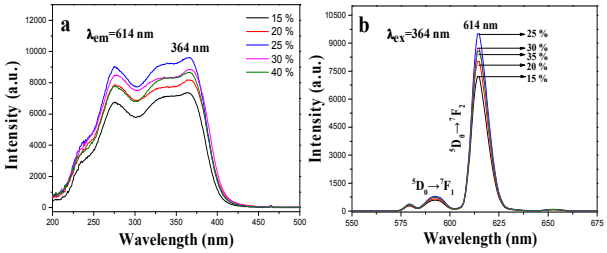

Fig. 5 Excitation spectra (a) and emission spectra (b) of $Eu(TTA)_3(TPPO)_2/PVP$ composite nanofibers containing different mass percentage of $Eu(TTA)_3(TPPO)_2$ complex

Besides, the fluorescent properties of the $[Fe_3O_4/PANI/PVP]@[Eu(TTA)_3(TPPO)_2/PVP]$ nanocables with different PANI contents (S1@S6, S2@S6 and S3@S6) are also investigated. The mass ratio of Fe_3O_4 NPs to PVP is fixed at 1:1. As shown in Fig. 6(a, b), it is clearly observed that emission and excitation intensity decrease with the increase of the PANI content. From the UV-Vis absorption spectrum of PANI illustrated in Fig. 6c, it can be seen that the PANI can absorb visible light (400-760 nm) and much more easily absorb the ultraviolet light (< 400 nm). Moreover, as shown in Fig. 6c, a broad absorption peak around 614 nm is also observed, meaning that PANI absorbs red light much stronger. The exciting light and emitting light in the nanocables are absorbed by PANI, resulting in that the intensities of exciting light and emitting light are decreased, and the light absorption becomes stronger with introducing more PANI into the nanocables.

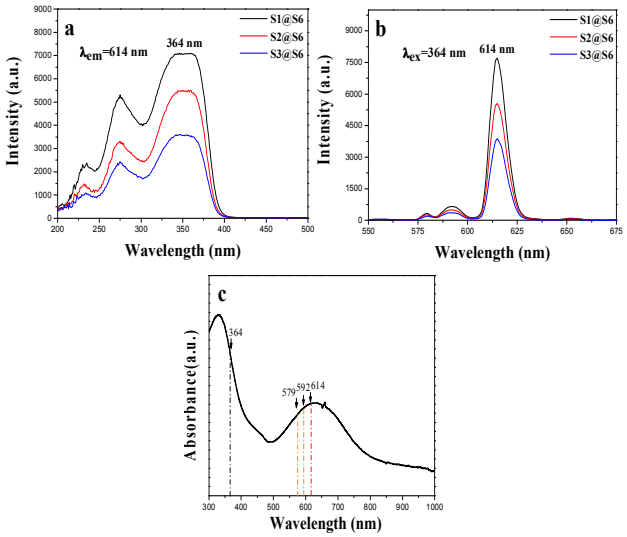

Fig. 6 Excitation spectra (a) and emission spectra (b) of the nanocables containing different mass percentages of PANI and UV-Vis absorbance spectrum (c) of PANI/PVP

Meanwhile, the $[Fe_3O_4/PANI/PVP]@[Eu(TTA)_3(TPPO)_2/PVP]$ nanocables containing different amounts of Fe_3O_4 NPs were fabricated to research the effect of adding different contents of Fe_3O_4 NPs (samples S2@S6, S4@S6, S5@S6, as illustrated in Fig. 7) on the fluorescent properties of the nanocables. Similarly, the excitation and emission intensity of nanocables are decreased with the increase of Fe_3O_4 NPs content. This phenomenon can be explained as the light absorption of Fe_3O_4 NPs. From the absorbance spectrum of Fe_3O_4 NPs illustrated in Fig. 7c, it is seen that the Fe_3O_4 NPs can absorb light at ultraviolet wavelength (< 400 nm) much more strongly than visible range (400-760 nm). The exciting light and emitting light in the nanocables are absorbed by Fe_3O_4 NPs, leading to the fact that the intensities of exciting light and emitting light are decreased, and the light absorption becomes stronger with introducing more Fe_3O_4 NPs into the nanocables.

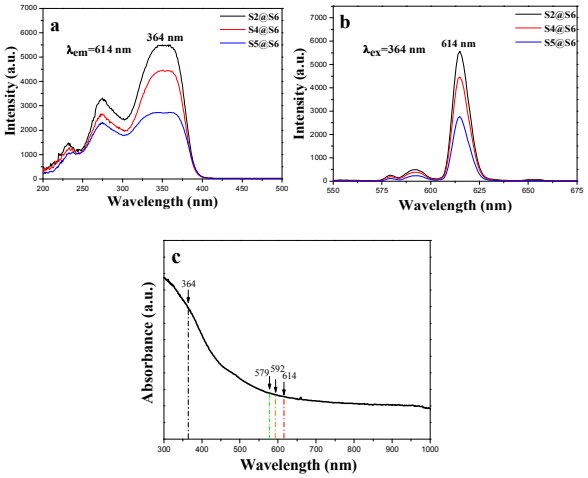

Fig. 7 Excitation spectra (a) and emission spectra (b) of the nanocables containing different mass percentages of Fe_3O_4 NPs and UV-Vis absorbance spectrum (c) of Fe_3O_4 NPs

From the contrast between the nanocables (S4@S6) and $Fe_3O_4/PANI/Eu(TTA)_3(TPPO)_2/PVP$ composite nanofibers with the same compositions, as shown in Fig. 8, one can see that excitation and emission intensity of the nanocables are much stronger than those of $Fe_3O_4/PANI/Eu(TTA)_3(TPPO)_2/PVP$ composite nanofibers. This result can be attributed to the isolation of $Eu(TTA)_3(TPPO)_2$ from Fe_3O_4 NPs and PANI. As illustrated in Fig. 9, $Eu(TTA)_3(TPPO)_2$, Fe_3O_4 NPs and PANI are evenly dispersed in the $Fe_3O_4/PANI/Eu(TTA)_3(TPPO)_2/PVP$ composite nanofiber. The exciting light in the composite nanofiber has to pass through Fe_3O_4 NPs and PANI to reach and excite $Eu(TTA)_3(TPPO)_2$. In this process, a large part of the exciting light has been absorbed by Fe_3O_4 NPs and PANI, and thus the exciting light is much weakened before it reaches the $Eu(TTA)_3(TPPO)_2$. Similarly, the emitting light emitted by

$Eu(TTA)_3(TPPO)_2$ also has to pass through Fe_3O_4 NPs and PANI and is absorbed by them**.** Consequently, both the exciting and emitting light are severely weakened. For the counterpart nanocables, Fe_3O_4 NPs and PANI are separated from $Eu(TTA)_3(TPPO)_2$ complexes in their own domains of the nanocables, so that the exciting light and emitting light in the $[Eu(TTA)_3(TPPO)_2/PVP]$ domain will almost be unaffected by Fe_3O_4 NPs and PANI. The overall result is that the nanocables possess much higher fluorescent performance than the Fe_3O_4/PANI/$Eu(TTA)_3(TPPO)_2$/PVP composite nanofibers. Thus, a strong fluorescent emission intensity of the nanocables is achieved by isolating $Eu(TTA)_3(TPPO)_2$ from Fe_3O_4 NPs and PANI.

Fig. 10 demonstrates the digital photos of Fe_3O_4/PANI/$Eu(TTA)_3(TPPO)_2$/PVP composite nanofibers (a) and [Fe_3O_4/PANI/PVP]@[$Eu(TTA)_3(TPPO)_2$/PVP] nanocables (S4@S6) (b). It is clearly observed that composite nanofibers present the black color and fragile character due to the direct existence of the dark-colored Fe_3O_4 NPs and PANI in all places of the composite nanofibers, while the color of the nanocables is close to white and more flexible owing to the fact that the dark-colored Fe_3O_4 NPs and PANI are existed only in the cores of the nanocables and the dark-colored Fe_3O_4/PANI/PVP cores are well coated by white-colored $Eu(TTA)_3(TPPO)_2$/PVP sheath. This result further proves that the well-defined nanocables are successully constructed via one-step specially designed coaxial spinnerets electrospinning technology. In addition, the color differences of the two samples further explain the reason why the fluorescent intensity of the nanocables are much stronger than the counterpart composite nanofibers.

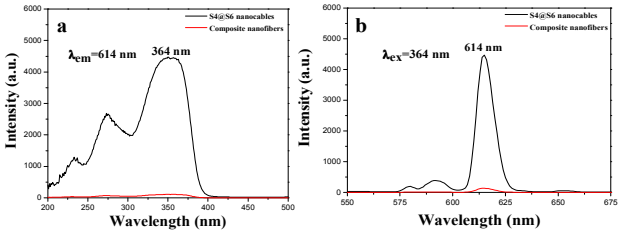

Fig. 8 Excitation spectra (a) and emission spectra (b) of the nanocables (S4@S6) and Fe_3O_4/PANI/$Eu(TTA)_3(TPPO)_2$/PVP composite nanofibers

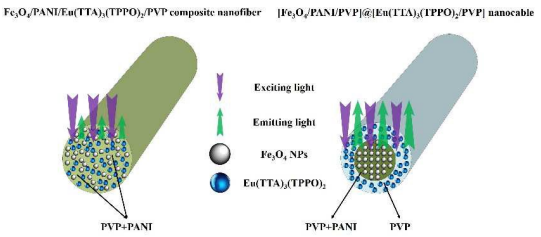

Fig. 9 Schematic diagrams of the situation of the exciting light and emitting light in the Fe_3O_4/PANI/$Eu(TTA)_3(TPPO)_2$/PVP composite nanofibers and [Fe_3O_4/PANI/PVP]@[$Eu(TTA)_3(TPPO)_2$/PVP] nanocables

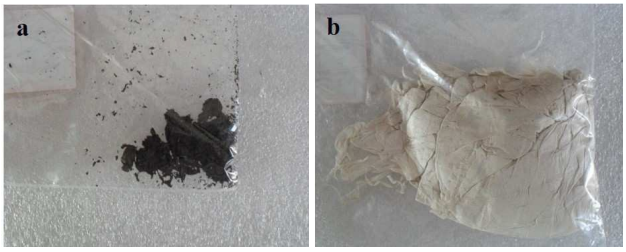

Fig. 10 Digital photos of Fe_3O_4/PANI/$Eu(TTA)_3(TPPO)_2$/PVP composite nanofibers (a) and [Fe_3O_4/PANI/PVP]@[$Eu(TTA)_3(TPPO)_2$/PVP] nanocables (S4@S6) (b) taken in natural light

3.3 Electrical conductivity analysis

As a result of conductive PANI only in the core of [Fe_3O_4/PANI/PVP]@[$Eu(TTA)_3(TPPO)_2$/PVP] nanocables, the nanocables are insulated from others. The electrical conductivity values of the cores we used for the [Fe_3O_4/PANI/PVP]@[$Eu(TTA)_3(TPPO)_2$/PVP] nanocables are summarized in Table 3 through measuring the dried spinning solution I-S1 (30 %), I-S2 (40 %) and I-S3 (50 %). The conductivities of the cores of these nanocables can be tuned by adjusting the mass percentage of PANI to PVP. Obviously, the more PANI introduced into the cores, the higher electrical conductivity of the cores, as PANI is consecutive in the Fe_3O_4/PANI/PVP nanofibers and probably forms the conducting network more easily, which render more efficient charge transport.

Table 3 Electrical conductivity and resistivity of the cores doped with various amount of PANI for the nanocables

Spinning solutions I	Conductivity ($S \cdot cm^{-1}$)	Resistivity ($\Omega \cdot cm$)
S1 (30 %)	4.65×10^{-3}	2.15×10^{2}
S1 (40 %)	8.50×10^{-3}	1.18×10^{2}
S1 (50 %)	1.08×10^{-2}	9.26×10^{1}

In order to investigate the insulativity of each nanocables, the surface conductivities of the nanocables (S1@S6, S2@S6 and S3@S6) were also measured by Hall effect measurement system, as summarized in Table 4. The results reveal that the surface conductivity of all the nanocables are lower than the order of 10^{-10} $S \cdot cm^{-1}$, indicating that the nanocables are well insulated.

Table 4 Electrical conductivity and resistivity of the nanocables doped with various amount of PANI as cores

Nanocables	Conductivity ($S \cdot cm^{-1}$)	Resistivity ($\Omega \cdot cm$)
S1@S6	1.41×10^{-10}	7.09×10^{9}
S2@S6	4.57×10^{-10}	2.19×10^{9}
S3@S6	6.13×10^{-10}	1.63×10^{9}

3.4 Magnetic property

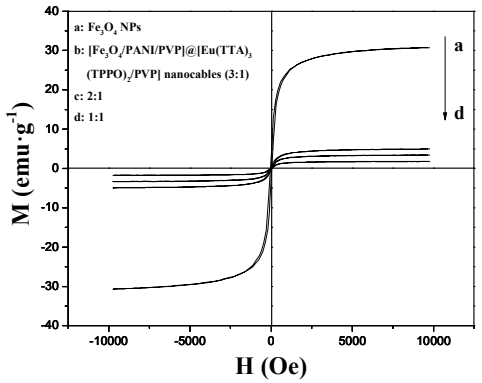

Fig. 11 Hysteresis loops of Fe_3O_4 NPs and [Fe_3O_4/PANI/PVP]@[$Eu(TTA)_3(TPPO)_2$/PVP] nanocables containing various mass percentages of Fe_3O_4 NPs

The typical hysteresis loops for Fe_3O_4 NPs and [Fe_3O_4/PANI/PVP]@[$Eu(TTA)_3(TPPO)_2$/PVP] nanocables containing various mass percentages of Fe_3O_4 NPs measured at room temperature are shown in Fig. 11, and the saturation magnetizations of the samples are listed in Table 5. It is a well-known fact that the saturation magnetization of a magnetic composite material depends on the mass percentage of the magnetic substance in the magnetic composite material. It is found from Table 5 that the saturation magnetization of the nanocables is increased from 1.76 emu·g^{-1} to 4.96 emu·g^{-1} with the increase of Fe_3O_4 NPs.

Table 5 Saturation magnetizations of Fe_3O_4 NPs and [Fe_3O_4/PANI/PVP]@[$Eu(TTA)_3(TPPO)_2$/PVP] nanocables

Samples	Saturation magnetization (Ms)/(emu·g^{-1})
Fe_3O_4 nanoparticles	30.76
[Fe_3O_4/PANI/PVP]@[$Eu(TTA)_3(TPPO)_2$/PVP] nanocables (Fe_3O_4:PVP=3:1)	4.96
[Fe_3O_4/PANI/PVP]@[$Eu(TTA)_3(TPPO)_2$/PVP] nanocables (Fe_3O_4:PVP=2:1)	3.39
[Fe_3O_4/PANI/PVP]@[$Eu(TTA)_3(TPPO)_2$/PVP] nanocables (Fe_3O_4:PVP=1:1)	1.76

4 Conclusions

In summary, uniform trifunctional luminescent-electrical-magnetic [Fe_3O_4/PANI/PVP]@[$Eu(TTA)_3(TPPO)_2$/PVP] nanocables were successfully prepared by coaxial electrospinning. The diameter of the nanocables is 414±13 nm. Fe_3O_4/PANI/PVP are successfully coated with $Eu(TTA)_3(TPPO)_2$/PVP complex. It is very gratifying to see that the nanocables simultaneously possess excellent luminescent performance, electrical conduction and magnetic properties. Furthermore, the luminescent intensity, electrical conductivity and magnetic properties of the nanocables can be tunable by adjusting contents of fluorescent compounds, PANI and Fe_3O_4 NPs, respectively. Besides, the design conception and preparation method of the coaxial nanostructure are of universal significance for the fabrication of other multifunctional nanomaterials such as electrical-magnetic, luminescent-electrical nanostructures.

Acknowledgements

This work was financially supported by the National Natural Science Foundation of China (NSFC 50972020, 51072026), Specialized Research Fund for the Doctoral Program of Higher Education (20102216110002, 20112216120003), the Science and Technology Development Planning Project of Jilin Province (Grant Nos. 20130101001JC, 20070402).

Notes and references

1 Y. R. Weng, J. Zhao, S. Y. Yu and S. Y. Song, *CrystEngComm*, 2014, **16**, 6257-6262.
2 Y. Gong, J. Dai, H. Li, X. Wang, H. Xiong, Q. Zhang, P. Li, C. Yi, Z. Xu, H. Xu and P. K. Chu, *J. Biomater. Appl.*, 2015, DOI: 10.1177/0885328215575761.
3 J. M. Rankin, N. K. Neelakantan, K. E. Lundberg, E. M. Grzincic, C. J. Murphy and K. S. Suslick, *Adv. Sci.*, 2015, DOI: 10.1002/advs.201500114.
4 J. M. Shen, X. M. Guan, X. Y. Liu, J. F. Lan, T. Cheng and H. X. Zhang, *Bioconjugate Chem.*, 2012, **23**, 1010-1021.
5 P. P. Yang, S. L. Gai and J. Lin, *Chem. Soc. Rev.*, 2012, **41**, 3679-3698.
6 S. Y. Yu, X. C. Gao, H. Jing, R. F. Zhang, X. L. Gao and H. Q. Su, *CrystEngComm*, 2014, **16**, 6645-6653.
7 P. C. Du, J. Zeng, B. Mu and P. Liu, *Mol. Pharmaceut.*, 2013, **10**, 1705-1715.
8 Y. T. Li, J. L. Tang, L. C. He, Y. Liu, Y. L. Liu, C. Y. Chen and Z. Y. Tang, *Adv. Mater.*, 2015, DOI: 10.1002/adma.201501779.
9 Y. Q. Wu, M. Shi, L. Z. Zhao, W. Feng, F. Y. Li and C. H. Huang, *Biomaterials*, 2014, **35**, 5830-5839.
10 Y. P. Shi, Y. Pan, J. Zhong, J. Yang, J. H. Zheng, J. L. Cheng, R. Song and C. Q. Yi, *Carbon*, 2015, **93**, 742-750.
11 H. Nishihara, *Chem. Lett.*, 2014, **43**, 388-395.
12 S. C. Wuang, K. G. Neoh, E. T. Kang, D. W. Pack and D. E. Leckband, *J. Mater. Chem.*, 2007, **17**, 3354-3362.
13 M. Bayat, H. Yang, F. K. Ko, D. Michelson and A. Mei, *Polymer*, 2014, **55**, 936-943.
14 X. Wang, D. P. Liu, S. Y. Song and H. J. Zhang, *Chem. Eur. J.*, 2013, **19**, 5169-5173.
15 T. M. Chan, Y. Y. Levitin, O. S. Kryskiv and I. A. Vedernikova, *J. Chem. Pharm. Res.*, 2015, **7**, 816-819.
16 G. Cheng, Z. G. Wang, Y. L. Liu, J. L. Zhang, D. H. Sun and J. Z. Ni, *ACS Appl. Mater. Interfaces*, 2013, **5**, 3182-3190.
17 D. Ling, N. Lee and T. Hyeon, *Acc. Chem. Res.*, 2015, **48**, 1276-1285.
18 R. Zhou, W. S. Liu, X. Y. Yao, Y. W. Leong and X. H. Lu, *J. Mater. Chem. A*, 2015, DOI: 10.1039/C5TA02154E.
19 D. Zhang, Y. L. Yin, C. H. Liu and S. S. Fan, *Chem. Commun.*, 2015, **51**, 322-325.
20 V. G. Pahurkar, Y. S. Tamgadge, A. B. Gambhire and G. G. Muley, *Sensor Actuat. B-Chem.*, 2015, **210**, 362-368.
21 D. H. Zhang and Y. Y. Wang, *Mater. Sci. Eng., B*, 2006, **134**, 9-19.
22 M. D. McGehee, T. Bergstedt, C. Zhang, A. P. Saab, M. B. O'Regan, G. C. Bazan, V. I. Srdanov and A. J. Heeger, *Adv. Mater.*, 1999, **11**, 1349-1354.

23 G. Shao, H. J. Yu, N. Zhang, Y. J. He, K. J. Feng, X. Yang, R. H. Cao and M. L. Gong, *Phys. Chem. Chem. Phys.*, 2014, **16**, 695-702.
24 F. Wang, W. B. Tan, Y. Zhang, X. P. Fan and M. Q. Wang, *Nanotechnology*, 2006, **17**, 1-3.
25 P. P. Sun, J. P. Duan, J. J. Lih and C. H. Cheng, *Adv. Funct. Mater.*, 2003, **13**, 683-691.
26 P. K. Shahi, A. K. Singh, S. B. Rai and B. Ullrich, *Sensor Actuat. A-Phys.*, 2015, **222**, 255-261.
27 S. J. Sheng, Q. L. Ma, X. T. Dong, N. Lv, J. X. Wang, W. S. Yu and G. X. Liu, *J. Mater. Sci.-Mater. Electron.*, 2014, **25**, 2279-2286.
28 S. Bharathkumar, M. Sakar, Rohith Vinod K and S. Balakumar, *Phys. Chem. Chem. Phys.*, 2015, DOI: 10.1039/c5cp01640a.
29 T. P. Cao, Y. J. Li, C. H. Wang, L. M. Wei, C. L. Shao and Y. C. Liu, *Mater. Res. Bull.*, 2010, **45**, 1406-1412.
30 W. Wang, Z. Y. Li, X. R. Xu, B. Dong, H. N. Zhang, Z. J. Wang, C. Wang, R. H. Baughman and S. L. Fang, *Small*, 2011, **7**, 597-600.
31 L. Han, Y. H. Hu, M. M. Pan, Y. F. Xie, Y. Y. Liu, D. Li and X. T. Dong, *CrystEngComm*, 2015, **17**, 2529-2535.
32 L. Han, M. M. Pan, Y. Lv, Y. T. Gu, X. F. Wang, D. Li, Q. L. Kong and X. T. Dong, *J. Mater. Sci.-Mater. Electron.*, 2015, **26**, 677-684.
33 F. Zhao, Q. F. Lu, S. W. Liu, C. F. Zhu and H. Y. Sun, *Mater. Lett.*, 2015, **139**, 19-21.
34 L. Y. Wang, X. T. Dong, G. Q. Gai, L. Zhao, S. Z. Xu and X. F. Xiao, *J. Nanopart. Res.*, 2015, **17**, 1-11.
35 Q. L. Ma, W. S. Yu, X. T. Dong, J. X. Wang, G. X. Liu and J. Xu, *J. Nanopart. Res.*, 2012, **14**, 1-7.
36 S. J. Sheng, Q. L. Ma, X. T. Dong, N. Lv, J. X. Wang, W. S. Yu and G. X. Liu, *Luminescence*, 2015, **30**, 26-31.
37 S. J. Sheng, Q. L. Ma, X. T. Dong, N. Lv, J. X. Wang, W. S. Yu and G. X. Liu, *J. Mater. Sci.-Mater. Electron.*, 2014, **25**, 1309-1316.
38 A. Zahoor, Q. Teng, H. Q. Wang, M. A. Choudhry and X. Y. Li, *Met. Mater. Int.*, 2011, **17**, 417-423.
39 S. Kumar, V. Kundu, A. Vohra and S. K. Chakarvarti, *J. Mater. Sci.-Mater. Electron.*, 2011, **22**, 995-999.
40 G. D. Qian, Z. Yang and M. Q. Wang, *J. Lumin.*, 2002, **96**, 211-218.
41 D. M. Chao, L. L. Cui, J. F. Zhang, X. C. Liu, Y. X. Li, W. J. Zhang and C. Wang, *Synth. Met.*, 2009, **159**, 537-540.

